AIAA JOURNAL
Vol. 37, No. 8, August 1999

Shape Design Optimization of Hyperelastic Structures Using a Meshless Method

Iulian Grindeanu,* Kyung K. Choi,† and Jiun-Shyan Chen‡
University of Iowa, Iowa City, Iowa 52242-1000
and
Kuang-Hua Chang§
University of Oklahoma, Norman, Oklahoma 73019

A shape design optimization procedure for hyperelastic structures is developed using a meshless method for analysis and a continuum-based design sensitivity analysis (DSA) method. The meshless method greatly reduces the mesh distortion or entanglement encountered in using the finite element method for large deformation nonlinear analysis and structural shape design optimization. The DSA method of Grindeanu et al. (Grindeanu, I., Chang, K.-H., Choi, K. K., and Chen, J.-S., "Design Sensitivity Analysis of Hyperelastic Structures Using a Meshless Method," *AIAA Journal*, Vol. 36, No. 4, 1998, pp. 618–627) is extended by using a pressure projection method to avoid volumetric locking for nearly incompressible materials without the need for large support sizes for the meshless shape functions and to reduce the CPU time. The Lagrange multiplier method is used to impose the essential boundary conditions. An engine mount is employed as an example to demonstrate the feasibility of the proposed optimization method. The mass is minimized subject to constraints on hydrostatic pressure and stiffness characteristics of the component. The design velocity fields corresponding to the shape design parameters are obtained using the Design Sensitivity Analysis and Optimization tool. Shape design optimization is carried out using the modified feasible direction of the Design Optimization Tool.

Nomenclature

a	= dilation parameter
$a({}^{t+\Delta t}\boldsymbol{z}, {}_0\bar{\boldsymbol{z}})$	= energy form
$a^*({}^t_0\boldsymbol{z}; {}_0\boldsymbol{z}, {}_0\bar{\boldsymbol{z}})$	= energy bilinear form
$C(\boldsymbol{x}; \boldsymbol{x}-\boldsymbol{s})$	= correction function
${}_0D_{ijkl}$	= incremental stress-strain tensor components
${}_0e_{ij}$	= linear part of incremental strain tensor components
${}^t_0F_{ij}$	= deformation tensor components, $\partial^t x_i/\partial X_j$ equals $\delta_{ij} + (\partial^t u_i/\partial X_j)$
$\boldsymbol{f}$	= external force
${}^t_0\boldsymbol{G}$	= right Cauchy–Green deformation tensor, $({}^t_0\boldsymbol{F})^T\,{}^t_0\boldsymbol{F}$
$\boldsymbol{H}$	= vector of monomials for definition of the reproducing kernel particle method shape functions
$\ell({}_0\bar{\boldsymbol{z}})$	= load form (virtual work done by external load), identical to ${}^{t+\Delta t}R$
$\boldsymbol{M}(\boldsymbol{x})$	= moment matrix of kernel function at $\boldsymbol{x}$
p	= hydrostatic pressure
${}_0S_{ij}$	= stress increments, ${}^{t+\Delta t}_0S_{ij} - {}^t_0S_{ij}$
${}^t_0S_{ij}$	= second Piola–Kirchhoff stress components
${}_0\boldsymbol{u}$	= incremental displacement vector, ${}^{t+\Delta t}_0\boldsymbol{u} - {}^t_0\boldsymbol{u}$
${}_0\bar{\boldsymbol{u}}$	= virtual displacement vector
${}^t_0\boldsymbol{u}$	= displacement vector, referred to the original configuration, ${}^t\boldsymbol{x} - \boldsymbol{X}$
${}^t_0W$	= strain energy density function
$\boldsymbol{X}$	= position of a material particle at initial configuration
${}^t\boldsymbol{x}$	= position of a material particle at time t
${}^t_0\boldsymbol{z}$	= vector of unknowns, $\{\boldsymbol{u}, \lambda^{s_u}, p\}$
${}^t\Gamma$	= domain boundary at time t
${}_0\varepsilon_{ij}$	= strain increments, ${}^{t+\Delta t}_0\varepsilon_{ij} - {}^t_0\varepsilon_{ij}$
${}^t_0\varepsilon_{ij}$	= Green–Lagrangian strain tensor components, $\frac{1}{2}({}^t_0G_{ij} - \delta_{ij})$
${}_0\eta_{ij}$	= nonlinear part of strain increments
λ	= Lagrange multiplier
Φ_a	= kernel function
$\bar{\Phi}_a(\boldsymbol{x}; \boldsymbol{x}-\boldsymbol{s})$	= modified kernel function
$\Psi_I(\boldsymbol{X})$	= interpolation function of particle $\boldsymbol{X}_I$, computed at $\boldsymbol{X}$
ψ	= performance measure
${}^t\Omega$	= physical domain at time t
$()'$	= first-order variation with respect to material property design variable u
$\dot{()}$	= total derivative with respect to shape design variable

Received 10 August 1998; revision received 1 January 1999; accepted for publication 20 January 1999.

*Research Assistant, Center for Computer-Aided Design and Department of Mechanical Engineering, College of Engineering; igrindea@ccad.uiowa.edu.

†Professor and Director, Center for Computer-Aided Design and Department of Mechanical Engineering, College of Engineering; kkchoi@ccad.uiowa.edu.

‡Assistant Professor, Center for Computer-Aided Design and Department of Mechanical Engineering, College of Engineering; jschen@icaen.uiowa.edu.

§Assistant Professor, School of Aerospace and Mechanical Engineering; khchang@ou.edu.

I. Introduction

FOR decades, the most successful numerical procedure for solving partial differential equations was the finite element analysis (FEA). As FEA technology was maturing, design optimization tools were developed based on FEA. Sizing, shape, configuration, and topology optimization problems were formulated and solved using FEA.

In shape design optimization, because the geometry of the structure is changing from an initial shape to an optimum shape, it is essential for the finite element meshes to vary smoothly from one iteration to another. Highly skewed finite elements or topologically different meshes can generate difficulties in computation of the design sensitivities and lead to instability of the overall optimization process. These problems that appear due to the finite element model were noticed relatively early.[1] Sophisticated automated mesh generation techniques,[2,3] careful choice of design variables,[4,5] and special techniques to obtain design velocity fields[6] were developed

and compared. Because the shape design remeshing cannot be done automatically, most of the time, the user has to intervene periodically during the optimization process. Shape optimization methodologies for p version of finite element analysis were proposed, and their advantages were discussed.[7–9]

Another approach for shape design sensitivity analysis (DSA) was proposed in Ref. 10. The analysis is performed using a new numerical technique called the reproducing kernel particle method (RKPM).[11–13] This numerical method belongs to a relatively new class of numerical procedures: the meshless (or mesh-free) methods. There are no fixed connectivities between the nodes in these methods, unlike the finite element or finite difference methods. They do require a set of nodes (particles) to discretize the domain, but do not require any prespecified connectivity of the nodes, or locally regular topological structure as is required in traditional meshing. These nodes can be generated automatically using a variety of schemes borrowed from traditional FEA, and the connection with CAD software packages is more direct and easier to establish.

An overview of the meshless methods developed in the recent years is presented in Ref. 14. For meshless methods, the Galerkin procedure is used in a way similar to FEA; the difference is that the shape functions that form the test and trial spaces are constructed using approximation methods such as moving least-squares approximation[15] or the reproducing kernel approximation.[11] These shape functions have a finite support, and they can be flexibly customized for desired regularity and completeness. In reproducing kernel approximation, for example, the exact reproduction of polynomials up to a specific order can be achieved by the appropriate enrichment of basis function in the approximation.

As the development of meshless methods progresses rapidly in complex mechanics problems,[16–19] there is a need for efficient design optimization tools tailored to these advances in computational mechanics. A very attractive feature in the meshless methods is its applicability to shape design optimization due to the absence of a mesh for constructing the shape functions; this unique property can greatly reduce the mesh distortion during design iterations.

In this paper, the Rivlin strain energy density function is employed to describe the hyperelastic structural behavior[20] and the Lagrange multiplier method is used for imposing essential boundary conditions.[14] One advantage of using meshless methods for incompressible problems is that the locking difficulty that exists in finite elements can be removed by simply increasing the support size of the meshless shape functions. This approach, however, considerably increases computational effort.

In the finite element context, the mixed formulations were used successfully for incompressible and nearly incompressible media.[20,21] Chen et al.[22,23] introduced the pressure projection finite element method as a generalization of the mixed formulation and selective reduced integration for nearly incompressible media and further extended it to the framework of the RKPM.[24]

Extensive work has been devoted lately to nonlinear design sensitivity analysis.[25–27] Choi and Duan[27] developed shape DSA and optimization methods for the hyperelastic structures using ABAQUS.[28] A mesh distortion problem, however, was encountered in the finite element analysis of an engine mount example using ABAQUS when a large load was applied.

The direct differentiation method was developed for material and shape design variables under the framework of the RKPM.[10] The DSA method of Ref. 10 is refined and extended here using the Lagrange multiplier method and a pressure projection method, and the resulting DSA methodology is applied for shape design optimization.

The remainder of the paper is organized as follows. Section II presents a variational equation of the hyperelastic structure and its linearized incremental form. Section III provides a brief overview for discretized form of the RKPM. Section IV describes the proposed material and shape DSA methods using RKPM. Section V presents shape design optimization of an engine mount to minimize the mass subject to constraints on hydrostatic pressure and stiffness characteristic of the component. A summary and future research directions are given in Sec. VI.

II. Variational Equations of Nonlinear Hyperelastic Structures

The total potential of hyperelasticity in the displacement based formulation, in conjunction with the Lagrange multiplier method for imposition of the essential boundary condition, is[22]

$$\Pi^*(\boldsymbol{u}, \lambda^{S_u}) = \int_\Omega W(\boldsymbol{u})\,\mathrm{d}\Omega - \int_\Omega u_i f_i^B\,\mathrm{d}\Omega - \int_{S_f} u_i f_i^{S_f}\,\mathrm{d}\Gamma - \int_{S_u} \lambda_i^{S_u}\left(u_i - u_i^p\right)\mathrm{d}\Gamma \tag{1}$$

where $W(\boldsymbol{u})$ is the strain energy density function for the nearly incompressible hyperelastic material:

$$W(\boldsymbol{u}) = \hat{W}(\hat{I}_1, \hat{I}_2) + \breve{W}(J) = \sum_{s+t\geq 1} A_{st}(\hat{I}_1 - 3)^s(\hat{I}_2 - 3)^t + \frac{k}{2}(J-1)^2 \tag{2}$$

where $\boldsymbol{u}$ is the displacement vector, λ^{S_u} are the Lagrange multipliers associated with the imposed essential boundary conditions, $\boldsymbol{f}^B$ is the externally applied body force, $\boldsymbol{f}^{S_f}$ is the surface traction, $\boldsymbol{u}^p$ is the prescribed displacement on surface S_u, k is the bulk modulus, and $\hat{I}_1$ and $\hat{I}_2$ are the reduced invariants. In Eq. (2),

$$\hat{W}(\hat{I}_1, \hat{I}_2) = \sum_{s+t\geq 1} A_{st}(\hat{I}_1 - 3)^s(\hat{I}_2 - 3)^t$$

is the strain energy density function that is associated with the reduced invariants, $\breve{W}(J) = (k/2)(J-1)^2$ is the hydrostatic work term in the strain energy function, and J is the determinant of the deformation gradient tensor. The reduced invariants are

$$\hat{I} = I_1 I_3^{-\frac{1}{3}} \tag{3a}$$

$$\hat{I}_2 = I_2 I_3^{-\frac{2}{3}} \tag{3b}$$

where

$$I_1 = \mathrm{tr}(\boldsymbol{G}) \tag{3c}$$

$$I_2 = \tfrac{1}{2}[\mathrm{tr}(\boldsymbol{G})^2 - \mathrm{tr}(\boldsymbol{G}^2)] \tag{3d}$$

$$I_3 = \det(\boldsymbol{G}) \tag{3e}$$

$$J = I_3^{\frac{1}{2}} = \det(\boldsymbol{F}) \tag{3f}$$

where $\boldsymbol{F}$ is the deformation gradient tensor and $\boldsymbol{G} = \boldsymbol{F}^T\boldsymbol{F}$ is the right Cauchy–Green deformation tensor. It is important to note that, in Eq. (1), the displacements and Lagrange multipliers associated with the essential boundary conditions are independent and can be interpolated separately in the discretization process.

By taking the stationary point of the total potential, the equilibrium equation at the configuration time $t + \Delta t$, with domain ${}^{t+\Delta t}\Omega$ and boundary ${}^{t+\Delta t}\Gamma$, can be obtained as

$$0 = \overline{\Pi^*(\boldsymbol{u}, \lambda^{S_u})} = \int_\Omega \bar{W}(\boldsymbol{u})\,\mathrm{d}\Omega - \int_\Omega \bar{u}_i f_i^B\,\mathrm{d}\Omega - \int_{S_f} \bar{u}_i f_i^{S_f}\,\mathrm{d}\Gamma - \int_{S_u} \bar{\lambda}_i^{S_u}\left(u_i - u_i^p\right)\mathrm{d}\Gamma - \int_{S_u} \lambda_i^{S_u}\bar{u}_i^{S_u}\,\mathrm{d}\Gamma \tag{4}$$

where the overbar represents the first-order variation of the quantity underneath. The first-order variation of the strain energy density function W can be obtained as

$$\bar{W}(\boldsymbol{u}) = {}^{t+\Delta t}_{0}S_{ij}\ {}^{t+\Delta t}_{0}\bar{\varepsilon}_{ij} \tag{5}$$

where the Piola–Kirchhoff stress tensor, the Green–Lagrange strain tensor, and its first-order variations are

$${}^{t+\Delta t}_{0}S_{ij} = \frac{\partial W(\boldsymbol{u})}{\partial\, {}^{t+\Delta t}_{0}\varepsilon_{ij}} = \frac{\partial \hat{W}}{\partial \hat{I}_n}\frac{\partial \hat{I}_n}{\partial\, {}^{t+\Delta t}_{0}\varepsilon_{ij}} + k(J-1)\frac{\partial J}{\partial\, {}^{t+\Delta t}_{0}\varepsilon_{ij}} \tag{6}$$

$$\begin{aligned} {}^{t+\Delta t}_{0}\varepsilon_{ij} &= \tfrac{1}{2}\left({}^{t+\Delta t}_{0}u_{i,j} + {}^{t+\Delta t}_{0}u_{j,i} + {}^{t+\Delta t}_{0}u_{k,i}\,{}^{t+\Delta t}_{0}u_{k,j}\right) \\ {}^{t+\Delta t}_{0}\bar{\varepsilon}_{ij} &= \tfrac{1}{2}\left({}_0\bar{u}_{i,j} + {}_0\bar{u}_{j,i} + {}_0\bar{u}_{k,i}\,{}^{t+\Delta t}_{0}u_{k,j} + {}^{t+\Delta t}_{0}u_{k,i}\,{}_0\bar{u}_{k,j}\right) \end{aligned} \tag{7}$$

In Eq. (6), the term $k(J-1)$, which can be interpreted as the hydrostatic pressure, causes numerical instability (volumetric locking) and pressure oscillation due to the large value of the bulk modulus k. Chen et al.[22–24] proposed the pressure projection method to overcome this difficulty. In this method, the hydrostatic pressure is projected onto a lower-order space, using the least-squares approximation procedure. That is, choose $\boldsymbol{p}^e = [p_1^e, p_2^e, \ldots, p_n^e]^T$ to minimize

$$\Phi(\boldsymbol{p}^e) = \|k(J-1) - \boldsymbol{Q}\boldsymbol{p}^e\|_{L_2}^2 = \int_\Omega (k(J-1) - \boldsymbol{Q}\boldsymbol{p}^e)^2 \, \mathrm{d}\Omega \quad (8)$$

where the L_2 norm is evaluated on a closed domain on which the projection space is defined. In Eq. (8), $\boldsymbol{Q}(x) = [Q_1(x), Q_2(x), \ldots, Q_n(x)]$ represents a basis for the projection space and the projected pressure $\tilde{p} = \boldsymbol{Q}\boldsymbol{p}^e$ is the approximation of the hydrostatic pressure in the least-squares sense. The minimization of Φ leads to

$$\int_\Omega \boldsymbol{Q}^T (k(J-1) - \boldsymbol{Q}\boldsymbol{p}^e) \, \mathrm{d}\Omega = \boldsymbol{0} \Leftrightarrow \int_\Omega \bar{\tilde{p}}(k(J-1) - \tilde{p}) \, \mathrm{d}\Omega = 0 \quad (9)$$

where $\bar{\tilde{p}}$ represents the first-order variation of the projected pressure.

The equilibrium equations are then obtained as

$$\int_\Omega {}^{t+\Delta t}_{0}S^*_{ij} \, {}_0\bar{\varepsilon}_{ij} \, \mathrm{d}\Omega - \int_{S_u} {}^{t+\Delta t}_{0}\lambda_i^{S_u} \bar{u}_i^{S_u} \, \mathrm{d}\Gamma = \int_\Omega \bar{u}_i f_i^B \, \mathrm{d}\Omega + \int_{S_f} \bar{u}_i^{S_f} f_i^{S_f} \, \mathrm{d}\Gamma - \int_{S_u} \bar{\lambda}_i^{S_u} \left({}^{t+\Delta t}_{0}u_i^{S_u} - u_i^p \right) \mathrm{d}\Gamma = 0 \quad (10)$$

$$\int_\Omega \bar{\tilde{p}} \left(k \left({}^{t+\Delta t}_{0}J - 1 \right) - {}^{t+\Delta t}_{0}\tilde{p} \right) \mathrm{d}\Omega = 0$$

where the stress tensor is computed by

$${}^{t+\Delta t}_{0}S^*_{ij} = \frac{\partial \hat{W}}{\partial \hat{I}_n} \frac{\partial \hat{I}_n}{\partial {}^{t+\Delta t}_{0}\varepsilon_{ij}} + {}^{t+\Delta t}_{0}\tilde{p} \frac{\partial J}{\partial {}^{t+\Delta t}_{0}\varepsilon_{ij}} \quad (11)$$

Note that in Eq. (8) the space described by the vector $\boldsymbol{Q}(x)$ has to be selected. Also, the norm that defines Φ can be selected, which leads to different integration scheme and, thus, to different projection methods. In this work, the pressure within each integration zone is assumed to be constant, and full integration is used in the pressure projection equation [Eq. (8)]. By choosing a full integration scheme in Eq. (8), the mixed displacement/pressure formulation proposed in Ref. 22 is obtained.

In mixed formulation, the total potential is augmented as

$$\Pi^*(\boldsymbol{u}, \tilde{p}, \lambda^{S_u}) = \int_\Omega W(\boldsymbol{u}, \tilde{p}) \, \mathrm{d}\Omega - \int_\Omega u_i f_i^B \, \mathrm{d}\Omega - \int_{S_f} u_i f_i^{S_f} \, \mathrm{d}\Gamma - \int_{S_u} \lambda_i^{S_u} \left(u_i - u_i^p \right) \mathrm{d}\Gamma \quad (12)$$

where

$$W(\boldsymbol{u}, \tilde{p}) = \hat{W}(\hat{I}_1, \hat{I}_2) + (k/2)(J-1)^2 - (1/2k)[k(J-1) - \tilde{p}]^2$$

and the pressure $\tilde{p}$ is viewed as an independent variable. If the reduced integration is used in Eq. (8), a selective reduced integration method for hyperelasticity can be obtained.

By the taking of the first-order variation in Eq. (12), the equilibrium equations can be obtained as

$$\int_\Omega {}^{t+\Delta t}_{0}S_{ij} \, {}_0\bar{\varepsilon}_{ij} \, \mathrm{d}\Omega - \int_{S_u} {}^{t+\Delta t}_{0}\lambda_i^{S_u} \bar{u}_i \, \mathrm{d}\Gamma = \int_\Omega \bar{u}_i f_i^B \, \mathrm{d}\Omega + \int_{S_f} \bar{u}_i f_i^{S_f} \, \mathrm{d}\Gamma$$
$$\int_\Omega \bar{\tilde{p}} \left({}^{t+\Delta t}_{0}J - 1 - \frac{{}^{t+\Delta t}_{0}\tilde{p}}{k} \right) \mathrm{d}\Omega = 0 \quad (13)$$
$$- \int_{S_u} \bar{\lambda}_i^{S_u} \left({}^{t+\Delta t}_{0}u_i - u_i^p \right) \mathrm{d}\Gamma = 0$$

These equations are the same as the equations in Eq. (10). By the denoting of the vector of unknowns $z = \{\boldsymbol{u}, \lambda^{S_u}, \tilde{p}\}$, the system of equations in Eq. (10) or Eq. (13) can be written in compact form as

$$a\left({}^{t+\Delta t}_{0}z, {}_0\bar{z} \right) \equiv \ell({}_0\bar{z}) \qquad \text{for all} \qquad {}_0\bar{z} \in {}_0z \quad (14)$$

To solve this nonlinear equation, the Newton–Raphson method is employed. The linearized incremental form of the equilibrium equation is introduced over the time interval $[t, t+\Delta t]$ as

$$\int_\Omega {}_0D_{ijkl} \, {}_0\bar{\varepsilon}_{ij} \, {}_0\varepsilon_{kl} \, \mathrm{d}\Omega + \int_\Omega {}^t_0S_{ij} \, {}_0\bar{\eta}_{ij} \, \mathrm{d}\Omega + \int_\Omega {}_0\tilde{p} \frac{\partial J}{\partial {}^t_0\varepsilon_{ij}} \, {}_0\bar{\varepsilon}_{ij} \, \mathrm{d}\Omega - \int_{S_u} {}_0\lambda_i^{S_u} \bar{u}_i^{S_u} \, \mathrm{d}\Gamma = \int_\Omega \bar{u}_i f_i^B \, \mathrm{d}\Omega + \int_{S_f} \bar{u}_i f_i^{S_f} \, \mathrm{d}\Gamma$$
$$- \left(\int_\Omega {}^t_0S_{ij} \, {}_0\bar{\varepsilon}_{ij} \, \mathrm{d}\Omega - \int_{S_u} {}^t_0\lambda_i^{S_u} \bar{u}_i \, \mathrm{d}\Gamma \right) \quad (15)$$
$$\int_\Omega \bar{\tilde{p}} \left(\frac{\partial {}^t_0J}{\partial {}^t_0\varepsilon_{kl}} \, {}_0\varepsilon_{kl} - \frac{{}_0\tilde{p}}{k} \right) \mathrm{d}\Omega = - \int_\Omega \bar{\tilde{p}} \left({}^t_0J - 1 - \frac{{}^t_0\tilde{p}}{k} \right) \mathrm{d}\Omega$$
$$\int_{S_u} \bar{\lambda}_i^{S_u} ({}_0u_i) \, \mathrm{d}\Gamma = - \int_{S_u} \bar{\lambda}_i^{S_u} \left({}^t_0u_i - u_i^p \right) \mathrm{d}\Gamma$$

where

$${}_0D_{ijkl} = \frac{\partial {}^t_0S_{ij}}{\partial {}^t_0\varepsilon_{kl}} = \frac{\partial^2 \hat{W}}{\partial \hat{I}_m \partial \hat{I}_n} \frac{\partial \hat{I}_m}{\partial {}^t_0\varepsilon_{ij}} \frac{\partial \hat{I}_n}{\partial {}^t_0\varepsilon_{kl}} + \frac{\partial \hat{W}}{\partial \hat{I}_m} \frac{\partial}{\partial {}^t_0\varepsilon_{kl}} \left(\frac{\partial \hat{I}_m}{\partial {}^t_0\varepsilon_{ij}} \right) + {}^t_0\tilde{p} \frac{\partial^2 J}{\partial {}^t_0\varepsilon_{ij} \partial {}^t_0\varepsilon_{kl}}$$

$${}_0\bar{\eta}_{ij} = \tfrac{1}{2} \left({}_0\bar{u}_{k,i} \, {}_0u_{k,j} + {}_0u_{k,i} \, {}_0\bar{u}_{k,j} \right)$$

$${}_0\varepsilon_{kl} = \tfrac{1}{2} \left({}_0u_{k,l} + {}_0u_{l,k} + {}^t_0u_{m,l} \, {}_0u_{m,k} + {}_0u_{m,l} \, {}^t_0u_{m,k} \right)$$

In Eq. (15), the unknowns are the incremental displacements ${}_0\boldsymbol{u}$, the incremental projected pressure ${}_0\tilde{p}$, and the incremental Lagrange multipliers ${}_0\lambda^{S_u}$. In compact form, the system of equations in Eq. (15) can be written as

$$a^*\left({}^t_0z; {}_0z, {}_0\bar{z} \right) = \ell(\bar{z}) - a\left({}^t_0z, {}_0\bar{z} \right) \qquad \text{for all} \qquad {}_0\bar{z} \in {}_0Z \quad (16)$$

where $\ell({}_0\bar{z})$ is the virtual work done by the external forces $\boldsymbol{f}^B$ and $\boldsymbol{f}^{S_f}$, and $a({}^t_0z, {}_0\bar{z})$ is the internal virtual work. Note that in Eq. (16) the external load is assumed to be deformation independent. It is also noted that the energy bilinear form $a^*({}^t_0z; {}_0z, {}_0\bar{z})$ is linear in both ${}_0z$ and ${}_0\bar{z}$.

III. RKPM

In the discrete form of RKPM,[11–13] the shape function Ψ_I corresponding to the particle I at the point $\boldsymbol{X} = \{X, Y\}$ is constructed using the formula

$$\Psi_I(\boldsymbol{X}) = C(\boldsymbol{X}, \boldsymbol{X} - \boldsymbol{X}_I) \Phi_a(\boldsymbol{X} - \boldsymbol{X}_I) \Delta V_I = \boldsymbol{H}^T(\boldsymbol{X} - \boldsymbol{X}_I) \boldsymbol{M}^{-1}(\boldsymbol{X}) \boldsymbol{H}(\boldsymbol{0}) \Phi_{a_I}(\boldsymbol{X} - \boldsymbol{X}_I) \Delta V_I \quad (17)$$

where $C(\boldsymbol{X}, \boldsymbol{X} - \boldsymbol{X}_I) \equiv \boldsymbol{H}^T(\boldsymbol{X} - \boldsymbol{X}_I) \boldsymbol{M}^{-1}(\boldsymbol{X}) \boldsymbol{H}(\boldsymbol{0})$ is a correction function,

$$\boldsymbol{H}(\boldsymbol{X} - \boldsymbol{X}_I) = \left\{ 1 \quad X - X_I \quad Y - Y_I \quad \cdots \quad (Y - Y_I)^n \right\}^T$$

is a vector that contains monomials up to the desired degree n, and $\Phi_{a_I}(\boldsymbol{X} - \boldsymbol{X}_I)$ is a nonnegative window function associated to particle I with support size a_r. The matrix $\boldsymbol{M}$ is

$$\boldsymbol{M}(\boldsymbol{X}) = \sum_{J=1}^{N} \boldsymbol{H}(\boldsymbol{X} - \boldsymbol{X}_J) \boldsymbol{H}(\boldsymbol{X} - \boldsymbol{X}_J)^T \Phi_{a_J}(\boldsymbol{X} - \boldsymbol{X}_J) \Delta V_J \quad (18)$$

The window functions Φ_{a_J} have finite supports, controlled by the dilation parameter a_J. Therefore, the sum in Eq. (18) does not need

to be performed for all of the particles $\boldsymbol{X}_J$, only the particles whose support covers $\boldsymbol{X}$ are involved in the computation

$$\boldsymbol{M}(\boldsymbol{X}) = \sum_{J \in P(X)} \boldsymbol{H}(\boldsymbol{X}-\boldsymbol{X}_J)\boldsymbol{H}(\boldsymbol{X}-\boldsymbol{X}_J)^T \Phi_{a_J}(\boldsymbol{X}-\boldsymbol{X}_J)\Delta V_J$$
$$P(\boldsymbol{X}) = \{\boldsymbol{J}, \|\boldsymbol{X}_J - \boldsymbol{X}\| < a_J\} \tag{19}$$

The shape functions in Eq. (17) have the differentiability order determined by the smoothness of the window functions Φ_{a_J}. The cubic B-spline is used for window function[10,13] so that the shape functions are C^2 continuous. It is easy to prove that the matrix $\boldsymbol{M}(\boldsymbol{X})$ is positive semidefinite: Let $\boldsymbol{v}$ be a vector with the same dimension as vector $\boldsymbol{H}$. It follows that

$$\boldsymbol{v}^T\boldsymbol{M}(\boldsymbol{X})\boldsymbol{v} = \boldsymbol{v}^T\left[\sum_{J \in P(X)} \boldsymbol{H}(\boldsymbol{X}-\boldsymbol{X}_J)\boldsymbol{H}(\boldsymbol{X}-\boldsymbol{X}_J)^T\Phi_{a_J}(\boldsymbol{X}-\boldsymbol{X}_J)\Delta V_J\right]\boldsymbol{v}$$
$$= \sum_{J \in P(X)} \boldsymbol{v}^T\boldsymbol{H}(\boldsymbol{X}-\boldsymbol{X}_J)\boldsymbol{H}(\boldsymbol{X}-\boldsymbol{X}_J)^T\boldsymbol{v}\Phi_{a_J}(\boldsymbol{X}-\boldsymbol{X}_J)\Delta V_J$$
$$= \sum_{J \in P(X)} \left[\boldsymbol{v}^T\boldsymbol{H}(\boldsymbol{X}-\boldsymbol{X}_J)\right]^2\Phi_{a_J}(\boldsymbol{X}-\boldsymbol{X}_J)\Delta V_J \geq 0 \tag{20}$$

For two-dimensional problems, with dimension of $\boldsymbol{H} = 3$ for linear consistency, a sufficient condition for $\boldsymbol{M}$ to be nonsingular is that the point $\boldsymbol{X}$ is covered by at least three supports of particles that are not collinear. Similar sufficient conditions can be found for higher dimension of $\boldsymbol{H}$ or three-dimensional problems. The space spanned by the shape functions defined in Eq. (17) has the so-called reproducing properties[11]; it exactly represents the polynomials up to the degree specified in the $\boldsymbol{H}$ vector.[13–15]

Let z^h and $\bar{z}^h$ be the approximations of z and $\bar{z}$, respectively. The RKPM interpolation functions for $\boldsymbol{u}^h$ and $\bar{\boldsymbol{u}}^h$ that are used in the Galerkin procedure are

$$u_i^h(\boldsymbol{X}) = \sum_{I=1}^{\mathrm{NP}} \Psi_I(\boldsymbol{X})d_{iI} \tag{21}$$

$$\bar{u}_i^h(\boldsymbol{X}) = \sum_{I=1}^{\mathrm{NP}} \Psi_I(\boldsymbol{X})\bar{d}_{iI} \tag{22}$$

where d_{iI} and $\bar{d}_{iI}$ are the generalized displacement and generalized virtual displacement of particle $\boldsymbol{I}$, respectively, and NP is the number of particles in the model.

The Lagrange multipliers associated with essential boundary conditions are interpolated using the collocation method, and the pressure is assumed constant over each integration zone (cell). At run time, pressure is condensed at the integration zone level.

IV. Design Sensitivity Analysis Using RKPM

The basic theory of DSA for meshless method presented in Ref. 10 is extended here, by using the Lagrange multiplier method and a pressure projection method.

A. Material Property Design Sensitivity Analysis

Consider the material property $\boldsymbol{b}$ as the design variable. Taking the derivative of the equilibrium equation Eq. (13) with respect to $\boldsymbol{b}$,

$$\int_\Omega {}_0C_{ijkl0}\bar{\varepsilon}_{ij}\varepsilon'_{kl}\,\mathrm{d}\Omega + \int_\Omega {}^t_0S_{ij}\bar{\eta}'_{ij}\,\mathrm{d}\Omega + \int_\Omega \tilde{p}'\frac{\partial J}{\partial {}^t_0\varepsilon_{ij}}{}_0\bar{\varepsilon}_{ij}\,\mathrm{d}\Omega$$
$$- \int_{S_u}\left(\lambda_i^{S_u}\right)'\bar{u}_i\,\mathrm{d}\Gamma = -\int_\Omega {}^t_0S'_{ij}\,{}_0\bar{\varepsilon}_{ij}\,\mathrm{d}\Omega$$
$$\int_\Omega \bar{\tilde{p}}\left(\frac{\partial^t_0 J}{\partial^t_0\varepsilon_{kl}}\varepsilon'_{kl} - \frac{\tilde{p}'}{k}\right)\mathrm{d}\Omega = -\int_\Omega \bar{\tilde{p}}\left(\frac{{}^t_0\tilde{p}}{k^2}\right)k'\,\mathrm{d}\Omega$$
$$- \int_{S_u}\bar{\lambda}_i^{S_u}(u_i)'\,\mathrm{d}\Gamma = 0 \tag{23}$$

where the prime denotes the derivative with respect to design parameter $\boldsymbol{b}$ and

$$\varepsilon'_{kl} = \tfrac{1}{2}\left(u'_{k,l} + u'_{l,k} + {}^{t+\Delta t}_0u_{m,l}u'_{m,k} + {}^{t+\Delta t}_0u_{m,k}u'_{m,l}\right)$$
$$\bar{\eta}'_{ij} = \tfrac{1}{2}\left({}_0\bar{u}_{k,i}u'_{k,j} + u'_{k,i}\,{}_0\bar{u}_{k,j}\right) \tag{24}$$

$${}^t_0S'_{ij} = \frac{\partial}{\partial b}\left({}^t_0S_{ij}\right) = \frac{\partial}{\partial b}\left(\frac{\partial W}{\partial {}^t_0\varepsilon_{ij}}\right) = \frac{\partial}{\partial {}^t_0\varepsilon_{ij}}\left(\frac{\partial W}{\partial b}\right)$$
$$= \frac{\partial}{\partial {}^t_0\varepsilon_{ij}}\left(\sum_{s+t\geq 1} A'_{st}(\hat{I}_1-3)^s(\hat{I}_2-3)^t + \frac{\tilde{p}^2}{2k^2}k'\right) \tag{25}$$

The system of equations in Eq. (23) can be written in compact form as[10]

$$a^*\left({}^t_0z; z', {}_0\bar{z}\right) \equiv \ell'_b({}_0\bar{z}) - a'_b\left({}^t_0z, {}_0\bar{z}\right) \qquad \text{for all} \qquad {}_0\bar{z} \in {}_0Z \tag{26}$$

The energy bilinear form on the left side of Eq. (26) is the same as in Eq. (16), but the system is solved now for the sensitivities z' with respect to material design variable $\boldsymbol{b}$.

B. Shape Design Sensitivity Analysis

The equilibrium equation for the perturbed shape design using the total Lagrangian formulation is[10]

$$a_{0\Omega_\tau}\left({}^{t+\Delta t}_0z, {}_0\bar{z}\right) = \ell_{0\Omega_\tau}({}_0\bar{z}) \qquad \text{for all} \qquad {}_0\bar{z} \in {}_0Z_\tau \tag{27}$$

The pointwise material derivative of the structural responses ${}^{t+\Delta t}_0z({}^0\boldsymbol{x})$ is[25,29]

$${}_0\dot{z}({}^0\boldsymbol{x}) = \lim_{\tau\to 0}\frac{{}^{t+\Delta t}_0z({}^0\boldsymbol{x}+\tau\boldsymbol{V}({}^0\boldsymbol{x})) - {}^t_0z({}^0\boldsymbol{x})}{\tau}$$
$$\equiv {}_0z'({}^0\boldsymbol{x}) + {}_0\nabla^t z^T\boldsymbol{V}({}^0\boldsymbol{x}) \tag{28}$$

By the taking of the total material derivative of Eq. (13) and rearranging so that the left side of these equations contain material derivative of independent variables, we obtain

$$\int_\Omega {}_0D_{ijkl0}\bar{\varepsilon}_{ij}\dot{\varepsilon}_{kl}\,\mathrm{d}\Omega + \int_\Omega {}^t_0S_{ij}\dot{\bar{\eta}}_{ij}\,\mathrm{d}\Omega + \int_\Omega \dot{\tilde{p}}\frac{\partial J}{\partial {}^t_0\varepsilon_{ij}}{}_0\bar{\varepsilon}_{ij}\,\mathrm{d}\Omega$$
$$- \int_{S_u}\left(\dot{\lambda}_i^{S_u}\right)\bar{u}_i\,\mathrm{d}\Gamma = -\int_\Omega {}_0D_{ijkl0}\bar{\varepsilon}_{ij}\varepsilon^V_{kl}\,\mathrm{d}\Omega$$
$$- \int_\Omega {}^t_0S_{ij}\,{}_0\bar{\varepsilon}_{ij}\,\mathrm{div}\,\boldsymbol{V}\,\mathrm{d}\Omega - \int_\Omega {}^t_0S_{ij}\bar{\eta}^V_{ij}\,\mathrm{d}\Omega$$
$$+ \int_\Omega \bar{u}_i f_i^B\,\mathrm{div}\,\boldsymbol{V}\,\mathrm{d}\Omega + F\left({}^t_0\boldsymbol{u}, \dot{\bar{\boldsymbol{u}}}\right) \tag{29}$$
$$\int_\Omega \bar{\tilde{p}}\left(\frac{\partial^t_0 J}{\partial^t_0\varepsilon_{kl}}\dot{\varepsilon}_{kl} - \frac{\dot{\tilde{p}}}{k}\right)\mathrm{d}\Omega = -\int_\Omega \bar{\tilde{p}}\left(\frac{\partial^t_0 J}{\partial^t_0\varepsilon_{kl}}\varepsilon^V_{kl}\right)$$
$$+ \bar{\tilde{p}}\left({}^t_0J - 1 - \frac{\tilde{p}}{k}\right)\mathrm{div}\,\boldsymbol{V}\,\mathrm{d}\Omega - \int_{S_u}\bar{\lambda}_i^{S_u}(\dot{u}_i)\,\mathrm{d}\Gamma = 0$$

where

$$\frac{\mathrm{d}}{\mathrm{d}\tau}\left({}^t_0\varepsilon_{ij}\right) = \frac{\mathrm{d}}{\mathrm{d}\tau}\left[\frac{1}{2}\left({}^t_0u_{i,j} + {}^t_0u_{j,i} + {}^t_0u_{k,i}\,{}^t_0u_{k,j}\right)\right]$$
$$= \frac{1}{2}\left[\frac{\mathrm{d}}{\mathrm{d}\tau}\left({}^t_0u_{i,j}\right) + \frac{\mathrm{d}}{\mathrm{d}\tau}\left({}^t_0u_{j,i}\right) + {}^t_0u_{k,i}\frac{\mathrm{d}}{\mathrm{d}\tau}\left({}^t_0u_{k,j}\right)\right.$$
$$\left. + \frac{\mathrm{d}}{\mathrm{d}\tau}\left({}^t_0u_{k,i}\right){}^t_0u_{k,j}\right] = \frac{1}{2}\left[\left(\dot{u}_{i,j} - u_{i,m}V^m_{,j}\right) + \left(\dot{u}_{j,i} - u_{j,m}V^m_{,i}\right)\right.$$
$$\left. + {}^t_0u_{k,i}\left(\dot{u}_{k,j} - u_{k,m}V^m_{,j}\right) + \left(\dot{u}_{k,i} - u_{k,m}V^m_{,i}\right){}^t_0u_{k,j}\right]$$
$$= \frac{1}{2}\left(\dot{u}_{i,j} + \dot{u}_{j,i} + {}^t_0u_{k,i}\dot{u}_{k,j} + \dot{u}_{k,i}{}^t_0u_{k,j}\right)$$
$$+ \frac{1}{2}\left[-u_{i,m}V^m_{,j} - u_{j,m}V^m_{,i} + {}^t_0u_{k,i}\left(-u_{k,m}V^m_{,j}\right)\right.$$
$$\left. + \left(-u_{k,m}V^m_{,i}\right){}^t_0u_{k,j}\right] \overset{\text{def}}{=} \dot{\varepsilon}_{ij} + \varepsilon^V_{ij}$$

$$\frac{\mathrm{d}}{\mathrm{d}\tau}({}_0\bar{\varepsilon}_{ij}) = \frac{1}{2}\left(\dot{u}_{k,i} - u_{k,m}V^m_{,i}\right){}_0\bar{u}_{k,j} + \frac{1}{2}\left(\dot{u}_{k,j} - u_{k,m}V^m_{,j}\right){}_0\bar{u}_{k,i}$$
$$+ \frac{\mathrm{d}}{\mathrm{d}\tau}\left[\frac{1}{2}({}_0\bar{u}_{i,j} + \bar{u}_{j,i})\right] + \frac{1}{2}\left[\frac{\mathrm{d}}{\mathrm{d}\tau}({}_0\bar{u}_{k,j}){}^t_0u_{k,i} + \frac{\mathrm{d}}{\mathrm{d}\tau}({}_0\bar{u}_{k,i}){}^t_0u_{k,j}\right]$$
$$= \frac{1}{2}(\dot{u}_{k,i}){}_0\bar{u}_{k,j} + \frac{1}{2}(\dot{u}_{k,j}){}_0\bar{u}_{k,i} + \frac{1}{2}\left(-u_{k,m}V^m_{,i}\right){}_0\bar{u}_{k,j}$$
$$+ \frac{1}{2}\left(-u_{k,m}V^m_{,j}\right){}_0\bar{u}_{k,i} + \frac{\mathrm{d}}{\mathrm{d}\tau}\left[\frac{1}{2}({}_0\bar{u}_{i,j} + {}_0\bar{u}_{j,i})\right]$$
$$+ \frac{1}{2}\left[\frac{\mathrm{d}}{\mathrm{d}\tau}\left({}_0\bar{u}_{k,j}\right){}^t_0u_{k,i} + \frac{\mathrm{d}}{\mathrm{d}\tau}({}_0\bar{u}_{k,i}){}^t_0u_{k,j}\right] \overset{\text{def}}{=} \dot{\bar{\eta}}_{ij} + \bar{\eta}^V_{ij} \qquad (30)$$

As before, the system of Eqs. (30) can be written in a compact form as

$$a^*\left({}^t_0z; \dot{z}, {}_0\bar{z}\right) \equiv a'_V\left({}^t_0z, {}_0\bar{z}\right) + \ell'_V(\dot{\bar{z}}) - a\left({}^t_0z, {}_0\dot{\bar{z}}\right), \quad \text{for all} \quad {}_0\bar{z} \in {}_0Z \qquad (31)$$

The right-hand side of the equation depends on the design velocity fields and on the final equilibrium solution. Thus, it can be evaluated after the final equilibrium configuration of nonlinear analysis is obtained. The bilinear form on the left-hand side is the same as in Eq. (16). Consequently, the stiffness matrix decomposed at the final equilibrium configuration can be reused to solve the sensitivity equation Eq. (31).

V. Shape Design Optimization of an Engine Mount

An engine mount with imposed displacement boundary conditions is modeled as a two-dimensional problem, shown in Fig. 1. The geometric model is created using MSC/PATRAN.[30] Because of symmetry, only half of the structure is analyzed. This half-model contains 206 particle points and 151 integration zones. The Mooney–Rivlin model is employed to describe the hyperelastic material, with material constants $A_{10} = 13.874$ N/cm^2 and $A_{01} = 5.933$ N/cm^2 and bulk modulus $k = 659920$ N/cm^2. The exterior boundary is fixed. The interior metal block (the shaded region in Fig. 1) is treated as a rigid body, and the stiffness of the mount is selected as a performance measure. The stiffness is computed by the ratio of the reaction force developed at the final load step and the prescribed displacement. The hydrostatic pressures at critical points are also selected as performance measures. In the following discussions, the hydrostatic pressure is expressed in newtons per square centimeter and the external force is expressed in newtons.

The analysis is carried out in 25 load steps, due to high nonlinearity of the model and large structural deformation. The maximum displacement prescribed at the final step is 1.397 cm. Figure 2 shows the fringe plot of the hydrostatic pressure on the deformed structure. The pressure projection method is used such that the hydrostatic pressure is assumed constant within each integration zone. Therefore, the hydrostatic pressure can be condensed at the integration zone level. A 3×3 Gaussian integration scheme is used for evaluation of the integrals over each cell. The load-displacement response of the engine mount at the initial design is shown in Fig. 3.

For the problem, 20 shape design parameters are selected: the x and y coordinates of 10 control points on the boundary as shown in Fig. 4. By the use of the boundary displacement method

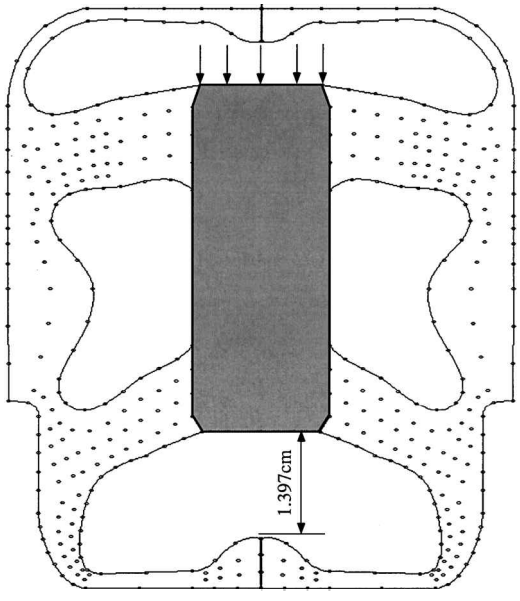

Fig. 1 Geometric model.

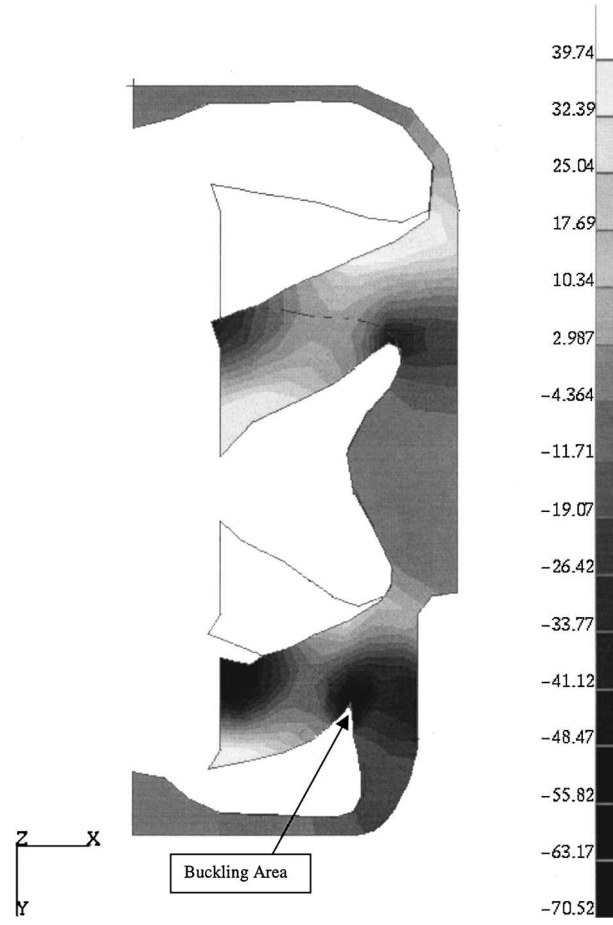

Fig. 2 Pressure fringe plot at final load step of initial design.

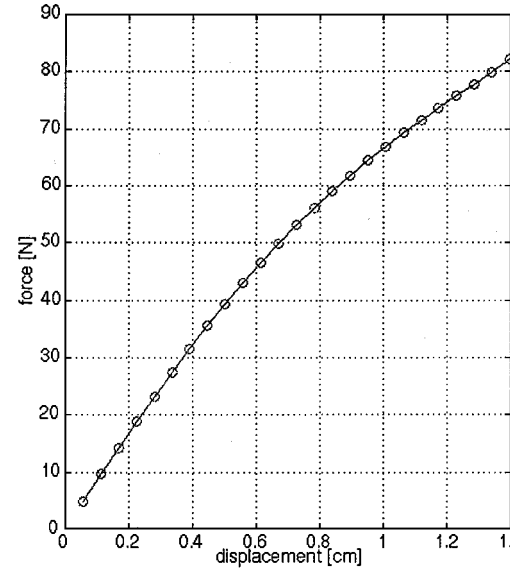

Fig. 3 Stiffness of engine mount: initial design.

Table 1 Verification of accuracy of design sensitivity

Performance	$\psi(\tau)$	$\psi(\tau+\delta\tau)$	$\delta\psi$	$d\psi/d\tau$	$\psi'/\delta\psi$
External force	82.2544969	82.2534566	−0.0010403	−10.59603	101.8547
Pressure, 19	−17.8374792	−17.8394391	−0.0019599	−19.5835417	99.9179
Pressure, 22	−10.609401	−10.6103983	−0.0009964	−10.09913	101.3481
Pressure, 38	−73.9683870	−73.971686	−0.0032996	−33.2033864	100.6285
Pressure, 39	−67.064370	−67.062390	0.00197976	19.7791618	99.9069

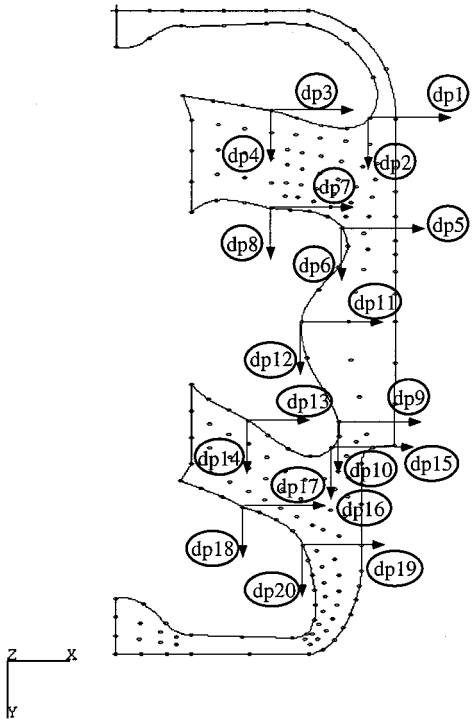

Fig. 4 Design parametrization.

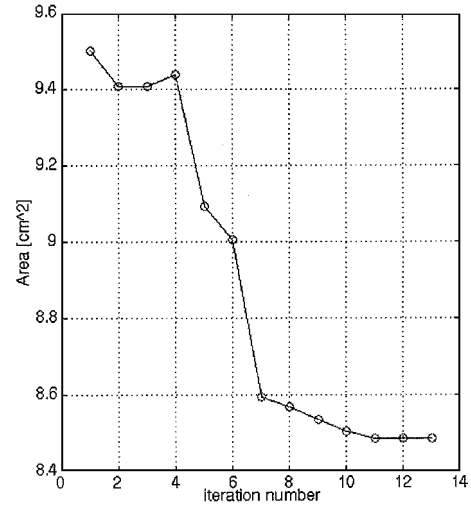

Fig. 5 Cost history.

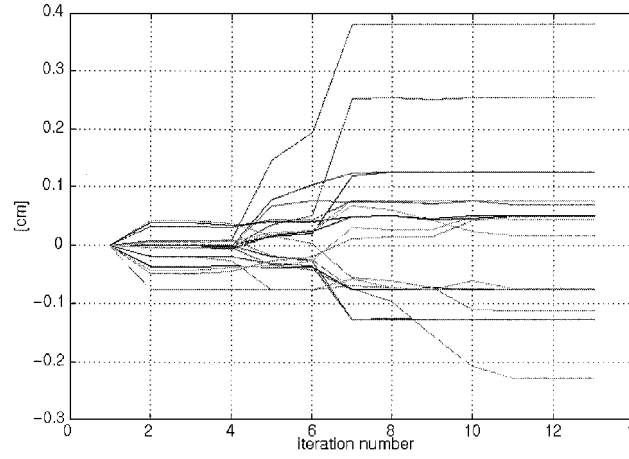

Fig. 6 Design parameters history.

provided in the Design Sensitivity Analysis and Optimization Tool,[5] 20 corresponding design velocity fields are computed. An auxiliary elastic model was employed to determine the domain velocity fields after the boundary velocity fields were computed using the MSC/PATRAN[30] cubic representation of each segment of the boundary.[5]

The sensitivity results are verified using the overall forward finite differences with perturbation of $1.E-4$ cm for design parameter 15, as shown in Table 1. In Table 1, $\psi(\tau)$ and $\psi(\tau+\delta\tau)$ are the performance measures at the current and perturbed designs, $\delta\psi$ is the finite difference, $\mathrm{d}\psi/\mathrm{d}\tau$ is the shape design sensitivity of performance measure ψ with respect to shape design parameter 15, and $\psi' = (\mathrm{d}\psi/\mathrm{d}\tau)\times\delta\tau$ is the predicted perturbation using the computed design sensitivities. The accuracy of the sensitivities is measured by the ratio in percentage between the finite difference and predicted perturbation $\Psi'/\delta\Psi$. As it can be seen in Table 1, the design sensitivity results are very accurate.

For design optimization, the amount of rubber material in the structure is selected as the cost function, for minimization. Two types of constraints are considered: the hydrostatic pressure and the external force. At the initial design, the lower arm experiences a localized buckling, as shown in Fig. 2. To avoid localized buckling, the magnitude of hydrostatic pressure is forced to be lower than 66 N/cm^2 at this hot spot, indicated in Fig. 2. At the initial design, this constraint is violated. Another constraint is that the optimum design is required to satisfy a given displacement–external force relationship to provide a specific stiffness. In this design problem, the stiffness characteristic of the original design (given in Fig. 3) is used as a constraint. The requirement imposed is that the ratio between the external force and the total displacement does not vary more than 3% for the optimum design, with respect to the initial design.

To summarize, the optimization problem is as follows: 1) minimize area (implicitly mass) of the rubber component, 2) subject to |pressure| < 66 N/mm^2:

$$-0.03 \le \frac{\text{current stiffness} - \text{initial stiffness}}{\text{initial stiffness}} \le 0.03$$

The optimization is carried out using the modified feasible design method available in the Design Optimization Tool (DOT).[31] The meshless model is updated at each step during the line search, for each iteration, and a complete analysis is carried to determine the objective and the constraints functions. The DSA information is requested by the DOT to compute a new search direction and to decide if the optimum point is reached.

The optimization process converged after 13 iterations. The cost function history, design parameter history, and normalized constraints history are shown in Figs. 5–7, respectively. The final shape of the structure is shown in Fig. 8. The pressure contour plot at optimum design is shown in Fig. 9, and the stiffness characteristic is shown in Fig. 10. The optimum design is compared with the initial design in Table 2.

Table 2 Cost and constraints functions for initial and optimum designs

Function	Initial design	Optimum design	Change, %
Cost (area), cm^2	9.501	8.445	−11.11
Stiffness, N/cm	58.88	57.05	−3.108
Pressure, 38, N/mm^2	−73.968	−65.989	10.78
Pressure, 39, N/mm^2	−67.064	−66.165	1.34

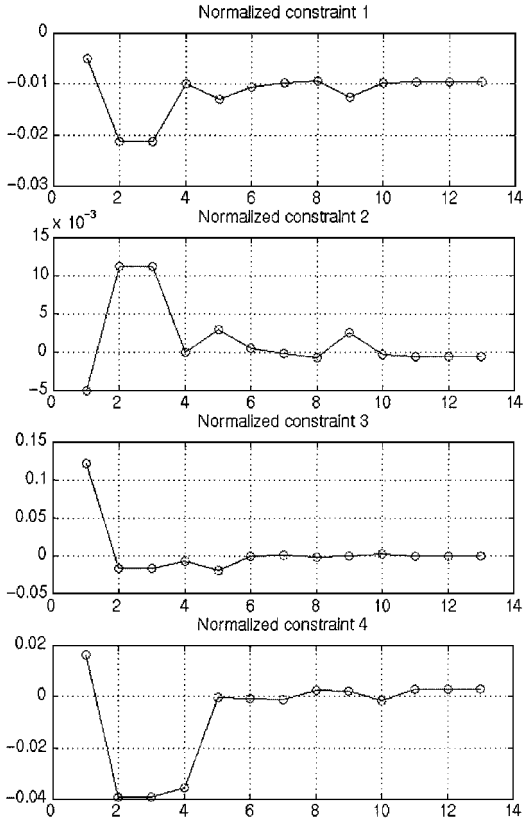

Fig. 7 Constraints history.

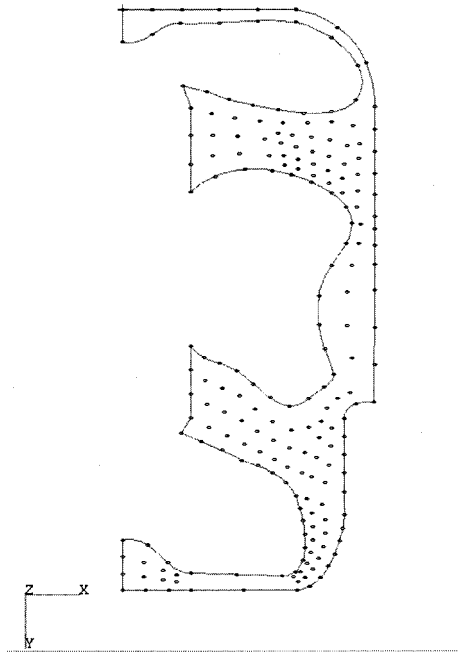

Fig. 8 Optimum design shape.

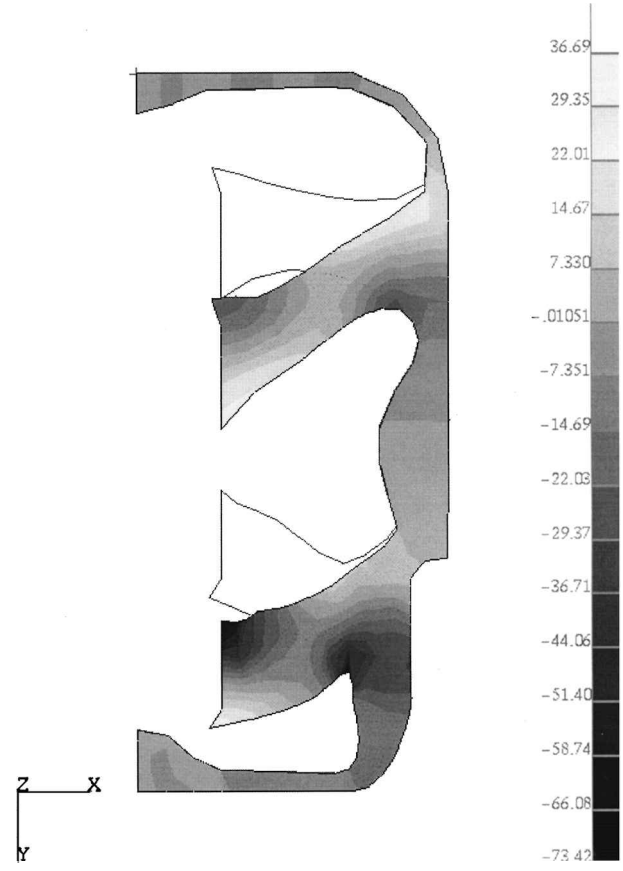

Fig. 9 Pressure contour plot at optimum design.

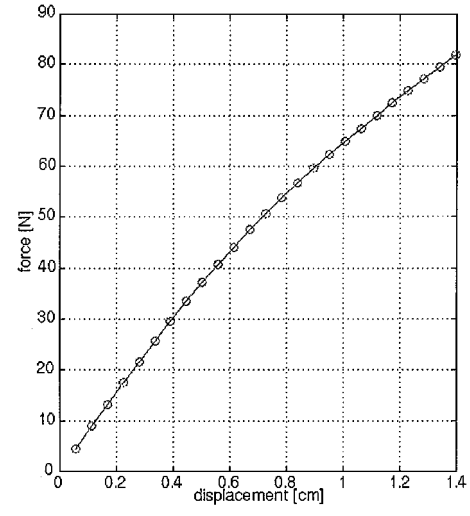

Fig. 10 Stiffness characteristic at the optimum design: final design.

VI. Conclusions

A continuum-based DSA and optimization method for hyperelastic structures using RKPM was presented. Both the material property and shape DSA methods for hyperelastic structures were extended to take advantage of the pressure projection method and the Lagrange multiplier method. The proposed optimization method was demonstrated to be effective using an engine mount example. Shape DSA and optimization using the meshless methods hold a great potential to eliminate mesh distortion problems that occur using traditional finite element methods. Currently, extension to three-dimensional problems, contact problems, and elastoplastic problems are being investigated. Also, a CAD-based optimization procedure for meshless methods is under development.

Acknowledgment

This research was supported by the U.S. Army Tank Automotive Command through the Automotive Research Center (DAAE07-94-C-R094).

References

[1]Haftka, R. T., and Grandhi, R. V., "Structural Shape Optimization—A Survey," *Computer Methods in Applied Mechanics and Engineering*, Vol. 57, No. 1, 1986, pp. 91–106.

[2]Kodyalam, S., and Thanedar, P. B., "Some Practical Aspects of Shape Optimization and Its Influence on Intermediate Mesh Refinement," *Finite Elements in Analysis and Design*, Vol. 15, No. 2, 1993, pp. 125–133.

[3]Banichuk, N. V., Barthold, F.-J., Falk, A., and Stein, E., "Mesh Refinement for Shape Optimization," *Structural Optimization*, Vol. 9, No. 1, 1995, pp. 46–51.

[4]Zhang, W. H., Beckers, P., and Fleury, C., "A Unified Parametric Design Approach to Structural Shape Optimization," *International Journal for Numerical Methods in Engineering*, Vol. 38, No. 13, 1995, pp. 2283–2292.

[5]Chang, K. H., Choi, K. K., Tsai, C. S., Chen, C. J., Choi, B. S., and Yu, X., "Design Sensitivity Analysis and Optimization Tool (DSO) for Shape Design Applications," *Computing Systems in Engineering*, Vol. 6, No. 2, 1995, pp. 151–175.

[6]Choi, K. K., and Chang, K. H., "A Study on Velocity Field Computation for Shape Design Optimization," *Finite Elements in Analysis and Design*, Vol. 15, No. 4, 1994, pp. 317–341.

[7]Salagame, R. R., and Belegundu, A. D., "Shape Optimization with *p* Adaptivity," *AIAA Journal*, Vol. 33, No. 12, 1995, pp. 2339–2405.

[8]Hwang, H.-Y., Choi, K. K., and Chang, K. H., "Shape Design Sensitivity and Optimization Using p-Version Finite Element Analysis," *Mechanics in Structures and Machines*, Vol. 25, No. 1, 1997, pp. 103–137.

[9]Hwang, H.-Y., Choi, K. K., and Chang, K. H., "Second-Order Shape Design Sensitivity Using p-Version Finite Element Analysis," *Journal of Structural Optimization*, Vol. 14, No. 2–3, 1997, pp. 91–99.

[10]Grindeanu, I., Chang, K.-H., Choi, K. K., and Chen, J.-S., "Design Sensitivity Analysis of Hyperelastic Structures Using a Meshless Method," *AIAA Journal*, Vol. 36, No. 4, 1998, pp. 618–627.

[11]Liu, W. K., Jun, S., and Zhang, Y. F., "Reproducing Kernel Particle Methods," *International Journal for Numerical Methods in Engineering*, Vol. 20, No. 10, 1995, pp. 1081–1106.

[12]Liu, W. K., Jun, S., Li, S., Adee, J., and Belytschko, T., "Reproducing Kernel Particle Methods for Structural Dynamics," *International Journal for Numerical Methods in Engineering*, Vol. 38, No. 10, 1995, pp. 1655–1679.

[13]Chen, J. S., Pan, C., Wu, T. C., and Liu, W. K., "Reproducing Kernel Particle Methods for Large Deformation Analysis of Nonlinear Structures," *Computer Methods in Applied Mechanics and Engineering*, Vol. 139, Nos. 1–4, 1996, pp. 195–227.

[14]Belytschko, T., Krongauz, Y., Organ, D., Flemming, M., and Krysl, P., "Meshless Methods: An Overview and Recent Developments," *Computer Methods in Applied Mechanics and Engineering*, Vol. 139, Nos. 1–4, 1996, pp. 3–47.

[15]Lancaster, P., and Salkauskas, K., "Surfaces Generated by Moving Least Squares Methods," *Mathematics of Computation*, Vol. 37, No. 155, 1981, pp. 141–158.

[16]Belytschko, T., Lu, Y. Y., Gu, L., and Tabbara, M., "Element-Free Galerkin Methods for Static and Dynamic Fracture," *International Journal of Solids and Structures*, Vol. 32, No. 17, 1995, pp. 2547–2570.

[17]Liu, W. K., Hao, W., Chen, Y., Jun, S., and Gosz, J., "Multiresolution Reproducing Kernel Particle Methods," *Computational Mechanics*, Vol. 20, No. 4, 1997, pp. 295–309.

[18]Chen, J. S., Pan, C., Roque, C. M. O. L., and Wang, H.-P., "A Lagrangian Reproducing Kernel Particle Method for Metal Forming Analysis," *Computational Mechanics*, Vol. 22, No. 3, 1998, pp. 287–307.

[19]Chen, J. S., Rouque, C. M. O. L., Pan, C., and Button, S. T., "Analysis of Metal Forming Process Based on Meshless Method," *Journal of Materials Processing Technology*, Vol. 80–81, 1998, pp. 642–646.

[20]Bathe, K. J., *Finite Element Procedures*, Prentice–Hall, Englewood Cliffs, NJ, 1996, pp. 561–566.

[21]Sussman, T., and Bathe, K. J., "A Finite Element Formulation for Nonlinear Incompressible Elastic and Inelastic Analysis," *Computers and Structures*, Vol. 26, 1987, pp. 357–409.

[22]Chen, J. S., Pan, C., and Wu, C. T., "A Pressure Projection Method for Nearly Incompressible Rubber Hyperelasticity, Part I: Theory," *Journal of Applied Mechanics*, Vol. 63, No. 4, 1996, pp. 862–868.

[23]Chen, J. S., Pan, C., and Wu, C. T., "A Pressure Projection Method for Nearly Incompressible Rubber Hyperelasticity, Part II: Applications," *Journal of Applied Mechanics*, Vol. 63, No. 4, 1996, pp. 869–877.

[24]Chen, J. S., Yoon, S., Wang, H. P., and Liu, W. K., "An Improved Reproducing Kernel Particle Method for Nearly Incompressible Hyperelastic Solids," *Computer Methods in Applied Mechanics and Engineering* (to be published).

[25]Santos, J. L. T., and Choi, K. K., "Shape Design Sensitivity Analysis of Nonlinear Structural Systems," *Structural Optimization*, Vol. 4, No. 1, 1992, pp. 23–35.

[26]Tortorelli, D. A., "Sensitivity Analysis for Nonlinear Constrained Elastostatic Systems," *International Journal for Numerical Methods in Engineering*, Vol. 33, No. 8, 1992, pp. 1643–1660.

[27]Choi, K. K., and Duan, W., "Shape Design Sensitivity Analysis of Hyperelastic Solids," *The First World Congress of Structural and Multidisciplinary Optimization*, edited by N. Olhoff and G. I. N. Rozvany, Elsevier Science, Tarrytown, NY, 1996, pp. 421–428.

[28]*ABAQUS User's Manual*, Ver. 4.8, Hibbit, Karlsson, and Sorensen, Inc., Providence, RI, 1990.

[29]Haug, E. J., Choi, K. K., and Komkov, V., *Design Sensitivity Analysis of Structural Systems*, Academic, New York, 1985, pp. 180–200.

[30]*MSC/PATRAN User Manual*, Ver. 5.0, MacNeal–Schwendler Corp., Los Angeles, 1996.

[31]*DOT User Manual*, Ver. 4.0, VMA Engineering, Goleta, CA, 1993.

A. D. Belegundu
Associate Editor